JOURNAL OF CATALYSIS **151**, 407–419 (1995)

Carbon Monoxide Oxidation over Catalysts Prepared by *in Situ* Activation of Amorphous Gold–Silver–Zirconium and Gold–Iron–Zirconium Alloys

A. Baiker,*[,1] M. Maciejewski,* S. Tagliaferri,* and P. Hug†

Department of Chemical Engineering and Industrial Chemistry, Swiss Federal Institute of Technology, ETH-Zentrum, CH-8092 Zürich, Switzerland, and †Institute of Inorganic Chemistry, University of Zürich, CH-8057 Zürich, Switzerland

Received March 25, 1994; revised August 15, 1994

Amorphous metal alloys with the compositions (at.%) Au_5FeZr_{14} and Au_5AgZr_{14} have been used as precursors for the preparation of gold–zirconia–iron oxide and gold–silver–zirconia catalysts for low-temperature CO oxidation. The catalysts were prepared by *in situ* activation (oxidation) of the glassy metal alloys under CO oxidation conditions at 280°C. The structural and chemical changes occurring during the transformation of the precursor alloys to the active stable catalysts were followed by thermal analysis, X-ray diffraction, scanning electron microscopy, and X-ray photoelectron spectroscopy. When exposed to CO reaction conditions, the glassy metal alloys exhibited initially very little activity due to the very low surface area of the alloys (<0.02 m^2/g). The activity developed with time on stream reaching a steady state after complete oxidation of the alloys. The stable active catalyst derived from Au_5FeZr_{14} was made up of gold particles supported on zirconia in which the iron oxide was dispersed. The catalyst prepared from Au_5AgZr_{14} contained gold–silver particles supported on zirconia. The zirconia formed by oxidation of the zirconium constituent was present in both catalysts as a mixture of poorly crystalline monoclinic and tetragonal phases. Both catalysts were microporous with BET surface areas of 30 m^2/g (Au_5FeZr_{14}) and 45 m^2/g (Au_5AgZr_{14}). Kinetic tests performed in a continuous tubular microreactor in the temperature range from −20 to 50°C showed that both catalysts are highly active for CO oxidation at low temperature. CO oxidation rates increased considerably if the $CO:O_2$ ratio in the reactant feed was changed from stoichiometry (2:1) to conditions of excess oxygen (1:2).

INTRODUCTION

Compared to the other Group IB metals, gold has hitherto found relatively little application in heterogeneous catalysis. An excellent review on the use of gold in heterogeneous catalysis, covering research up to 1983, has been written by Schwank (1). It has been known for a long time that gold surfaces are capable of catalyzing the oxidation of carbon monoxide to carbon dioxide (2, 3). Paravano and co-workers studied extensively the redistribution of isotopic carbon between these two gases on supported gold catalysts (4, 5). They report that the nature of the support had a decisive influence on the catalytic activity of gold; magnesia- and alumina-supported gold were more active by greater than one order of magnitude for the oxygen transfer between CO and CO_2 than silica-supported gold (5). Cant and Fredrickson (6) studied the reactions of CO with O_2 and NO over gold and silver sponges. On gold, oxidation by oxygen was about 40 times faster than with nitric oxide. Haruta *et al.* (7, 8) prepared highly dispersed gold on various metal oxides by coprecipitation and deposition–precipitation. They found that gold supported on TiO_2, α-Fe_2O_3, Co_3O_4, NiO, $Be(OH)_2$, and $Mg(OH)_2$ is very active for low-temperature CO oxidation. For gold supported on TiO_2, α-Fe_2O_3, and Co_3O_4, the turnover frequencies for CO oxidation per gold atom were found to be almost independent of the kind of support oxides used and to increase sharply with a decrease in the diameter of the gold particles below 4 nm. Small gold particles were suggested to provide not only sites for the reversible adsorption of CO but also to increase the amount of oxygen adsorbed on the support oxide. Vannice and co-workers (9) studied CO oxidation over differently pretreated Au–TiO_2 and Au–SiO_2 catalysts. After a high-temperature reduction at 773 K, TiO_2-supported gold became very active for CO oxidation and was an order of magnitude more active at 313 K than SiO_2-supported Au. The high activity of the Au–TiO_2 catalyst was attributed to a synergistic interaction between gold and titania. More recently, we have studied the CO oxidation behaviour of gold–zirconia prepared by coprecipitation (10). Although this catalyst was highly active, it showed significant deactivation in long term tests. CO oxidation catalysts with good low-temperature activity

---

[1] To whom correspondence should be addressed.

0021-9517/95 $6.00

are not only valuable for environmental applications, but also find important use in orbiting CO_2 lasers (11) and CO detectors (12).

In the search for efficient and stable CO oxidation catalysts for low-temperature applications we have prepared zirconia-based gold catalysts by exposing amorphous Au_5FeZr_{14} and Au_5AgZr_{14} alloys to CO oxidation conditions at 280°C. In contrast to the gold–zirconia catalyst prepared by coprecipitation (10), the gold catalysts derived from these glassy alloys show stable long term activity. Here we report results concerning the preparation, structural properties, and catalytic behaviour of these catalysts.

EXPERIMENTAL

Catalyst Precursors

The amorphous Au_5FeZr_{14}, Au_5AgZr_{14}, and $PdZr_2$ alloys used as catalyst precursors were prepared from the premixed melt of the pure constituents by rapid quenching using the technique of melt spinning. Chemical bulk analysis by means of inductive coupled plasma (ICP) and X-ray fluorescence revealed that the final alloys contained traces (ppm level) of Hf, Cu, and Si besides the main constituents. For use in the catalytic tests, the 20–30-mm-thick ribbons fabricated by melt spinning were ground into flakes of 0.1—1 mm size under liquid nitrogen. The BET surface area of these materials measured by krypton adsorption amounted to 0.017 (Au_5FeZr_{14}), 0.013 m^2/g (Au_5AgZr_{14}), and 0.03 m^2/g ($PdZr_2$). X-ray analysis of the glassy metal alloys before and after grinding indicated that the grinding did not lead to crystallization of the materials.

Characterization

The precursor materials and the final catalysts were investigated with regard to their physical and chemical properties using powder X-ray diffraction (XRD), differential thermal analysis (DTA), thermogravimetry (TG), scanning electron microscopy combined with electron dispersive X-ray analysis (EDX), X-ray photoelectron spectroscopy (XPS), and nitrogen adsorption.

X-ray diffraction patterns were measured on a Siemens D5000 powder X-ray diffractometer. The diffractograms were recorded with detector-sided Ni-filtered Cu $K\alpha$ radiation over a 2θ-range of 20° to 80° and a position sensitive detector. The measured patterns were compared with JCPDS data files (13). Estimates of the mean gold crystallite sizes were made using the Scherrer equation and the widths of selected diffraction lines of gold ((111), (200), (220)), according to the procedure described in Ref. (14).

Thermoanalytical measurements (DTA, TG) were carried out on either a Mettler 2000C thermoanalyzer or a Netzsch STA 409 instrument using α-alumina as a reference. The DTA investigations of the crystallization processes of the alloys were carried out at a heating rate of 10 K/min under argon flowing at 30 cm^3/min (STP). The oxidation of the alloys was studied under flowing air (30 cm^3/min (STP)) with a five times lower heating rate (2 K/min) due to the large exothermicity of this process.

Scanning electron microscopy (SEM) studies were performed using a Philips SEM 515-microscope equipped with a Tracor EDX 5400 detector for energy dispersive X-ray analysis (EDX). The samples were sputter-coated with gold–palladium (90/10) for SEM and with carbon for EDX analysis.

X-ray photoelectron spectroscopy (XPS) investigations were carried out using a Kratos S800 XPS instrument. The energy scale was calibrated using Au $4f_{7/2} = 84.0$ eV. The spectrometer was operated at a constant pass energy of 40 eV which resulted in a resolution of 1.0 eV for Ag $3d_{5/2}$. The spectra were measured with Mg$K\alpha$ radiation at a pressure $<5 \times 10^{-9}$ mbar. The samples were pressed on an indium foil and investigated without further treatment.

BET surface areas were determined by adsorption of nitrogen (catalysts) or krypton (metal alloy precursors) at 77 K in the relative pressure range $0.05 < p/p_0 < 0.25$, assuming a cross-sectional area of 0.162 nm^2 for the nitrogen molecule and 0.200 nm^2 for the krypton atom. Nitrogen adsorption and desorption isotherms were measured with a Micromeritics ASAP 2000 instrument, whereas krypton adsorption measurements were carried out in a glass volumetric adsorption apparatus, equipped with a high precision pressure gauge (Ruska DDR 6000). Prior to the adsorption measurements, the samples were outgassed under vacuum at 423 K for 2 h.

Catalytic Tests

Kinetic measurements were carried out using an apparatus which consisted of a continuous fixed-bed reactor, a gas dosing system, and two IR spectrometers for analysis of CO and CO_2, respectively. The Pyrex glass reactor was 20 cm long and had an inner diameter of 0.4 cm; it was heated by a heating mantle connected to a temperature controller. The temperature in the catalyst bed was measured by a chromel–alumel thermocouple, which was inserted into the centre of the bed. The reactor temperature could be held constant to within ±1°C.

The reactor tube was charged with 0.3 g of the amorphous metal alloy precursor which, after the *in situ* oxidation, resulted in a catalyst bed of ca. 1.5 cm height.

Premixed gases were taken from pressurised gas cylinders without further purification. The mixtures were 5000 ppm CO (99.997%) in N_2 (99.999%) and 5000 ppm O_2 (99.999%) in N_2. All experiments were carried out at atmospheric pressure with a total gas flow rate of 150 $cm^3/$

min (STP). For the *in situ* activation (oxidation) of the alloy precursors, the partial pressures of the gaseous components (CO and O_2) were 0.17 kPa in a nitrogen balance, whereas for the standard feed composition used in the kinetic measurements a stoichiometric CO : O_2 mixture (2 : 1) was used, corresponding to 0.17 kPa CO and 0.085 kPa O_2, respectively. Prior to all kinetic tests, the activated (oxidized) alloys were reduced under a pure hydrogen stream (50 cm^3/min) raising the temperature from 25 to 300°C in 2 h. Afterwards this temperature was maintained for 2 h and then the catalyst was cooled under the hydrogen flow to room temperature. Finally, the catalysts were heated to 150°C under a nitrogen stream and kept under these conditions for 2 h to guarantee the decomposition of hydrides, which might have formed during the preceding hydrogen exposure.

Preliminary tests using different flow rates, but where the ratio of catalyst weight to molar flow rate was kept constant, indicated that the flow rate used (150 cm^3/min) in the kinetic tests was large enough to avoid any influences caused by interparticle mass and heat transfer limitations. Tests concerning possible intraparticle mass transfer influences could not be performed with the catalysts, since the particle size could not be varied in a sufficiently large range due to embrittlement of the materials.

In some experiments, the weight gain of the alloys during *in situ* oxidation was determined by rapid cooling (quenching) and subsequent weighing of the reactor at specified times. The temperature dependences of the CO oxidation rates (Arrhenius plots) were measured using both an ascending and a descending temperature sequence. At each temperature step, the reaction rates were measured after steady-state conversion had been achieved. In the kinetic measurements CO conversions were typically below 15% and the system was treated as a differential reactor.

Reaction rates were calculated using the relation $r = (F_{CO,in}-F_{CO,out})/W$, where $F_{CO,in}$ and $F_{CO,out}$ are the molar flow rates of CO at the reactor inlet and outlet, respectively, and W is the catalyst mass.

RESULTS

Morphological and Chemical Properties of Precursor Alloys and Active Catalysts

For preparing a metal–metal oxide catalyst from a glassy metal alloy, at least one component of the alloy has to be oxidized. The oxidation should be performed under conditions where the oxidation process is faster than the crystallization, since the glassy material is generally more reactive towards oxygen than its crystalline counterpart (15), thus allowing oxidation at relatively lower temperature. Consequently, information on the crystallization and oxidation behaviour of the alloys is crucial to control their transformations to the final active metal/metal oxide catalysts.

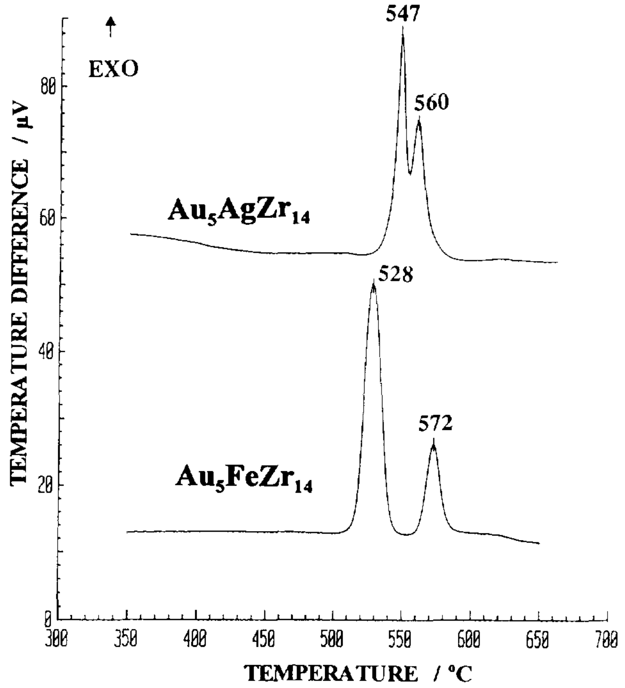

FIG. 1. Crystallization behaviour of amorphous Au_5AgZr_{14} and Au_5FeZr_{14} alloys investigated by DTA. Conditions: heating rate, 10°C/min; argon flow rate, 30 cm^3/min.

Figure 1 depicts the crystallization behaviour of the Au_5AgZr_{14} and Au_5FeZr_{14} glassy metal alloys used as catalyst precursors. The DTA curves measured under an argon atmosphere indicate that with both alloys, crystallization occurs in two discernible exothermal steps above 500°C. These steps are more distinctly separated with Au_5FeZr_{14}. However, both glassy metal alloys exhibit approximately similar thermal stability towards crystallization, as indicated by the DTA curves.

The oxidation behaviour of the glassy alloys in air, studied by TG combined with DTA, is illustrated in Fig. 2. The thermoanalytical measurements indicate that the oxidation of Au_5FeZr_{14} occurs considerably faster than that of Au_5AgZr_{14}. Note that with Au_5FeZr_{14}, oxidation started at a temperature as low as 125°C and reached a maximum at 265°C, whereas with Au_5AgZr_{14} the onset was observed at about 180°C and the maximum oxidation rate at 340°C. The weight gains calculated assuming that all constituents except gold are oxidized to the corresponding oxides (ZrO_2, Fe_2O_3, Ag_2O) are 19.2% for Au_5AgZr_{14} and 20.4% for Au_5FeZr_{14}. The measured weight gains of 18.3% and 20.1%, respectively, agree fairly well with these calculated values.

X-ray analysis of the bulk structure of the oxidized materials indicated that the solid was fully oxidized to a

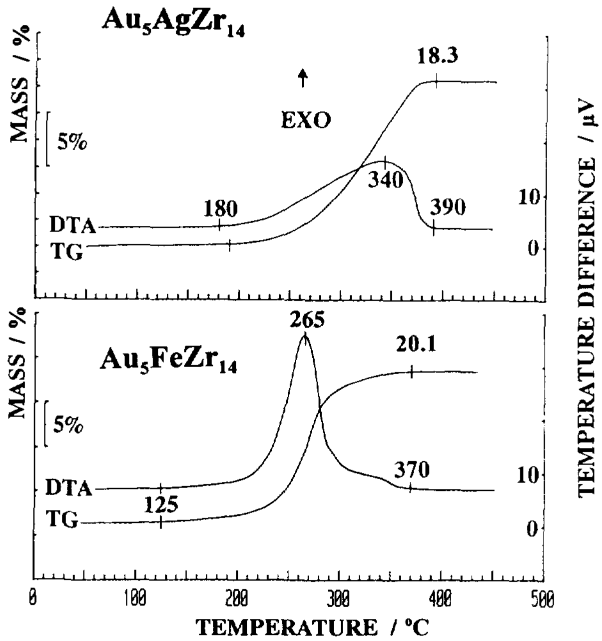

FIG. 2. Oxidation behaviour of amorphous Au$_5$AgZr$_{14}$ and Au$_5$FeZr$_{14}$ alloys investigated by DTA and TG. Conditions: heating rate, 2°C/min; air flow rate, 30 cm^3/min.

mixture of poorly crystalline tetragonal and monoclinic zirconia containing small gold crystallites. Silver- and iron-containing phases were not discernible in the XRD patterns due to the small amount of these constituents (5 at.%).

The preliminary studies of the crystallization and oxidation behaviour (Figs. 1 and 2) indicated that for the transformation of the glassy metal alloys to the gold–metal oxide catalysts a maximum temperature of less than 300°C should be applied in order to prevent thermal crystallization of the glassy material before its oxidation. Consequently, the *in situ* activation (oxidation) of the alloys was performed at 280°C.

When exposed to CO oxidation conditions at 280°C, the amorphous Au$_5$AgZr$_{14}$ and Au$_5$FeZr$_{14}$ alloys did not initially exhibit significant activity; the activity developed with the oxidation of the alloys by oxygen present in the reactant mixture. Figure 3 shows the development of the CO oxidation activities and the course of the oxidation of the alloys as a function of time-on-stream. The corresponding results found earlier for an amorphous PdZr$_2$ alloy (16) are also plotted in Fig. 3, for comparison. Note that upon exposure to CO oxidation conditions, the CO conversion activity of both gold-containing alloys developed at a slower rate than with similarly treated amorphous PdZr$_2$. A significant difference is also observed between the two gold-containing alloys; full activation is obtained significantly faster with Au$_5$FeZr$_{14}$ when compared to Au$_5$AgZr$_{14}$. The percentage weight gains due to oxidation of the alloys (plateaus in the gravimetric curves, Fig. 3.b) are about the same as those measured in the TG experiments (Fig. 2).

Figure 4 depicts the powder X-ray diffraction patterns of the amorphous metal alloy before and after *in situ* activation under CO oxidation conditions at 280°C. The patterns indicate that after activation both samples contained crystalline gold particles and a mixture of poorly crystalline monoclinic and tetragonal ZrO$_2$. The silver- and iron-containing phases were not detectable by XRD.

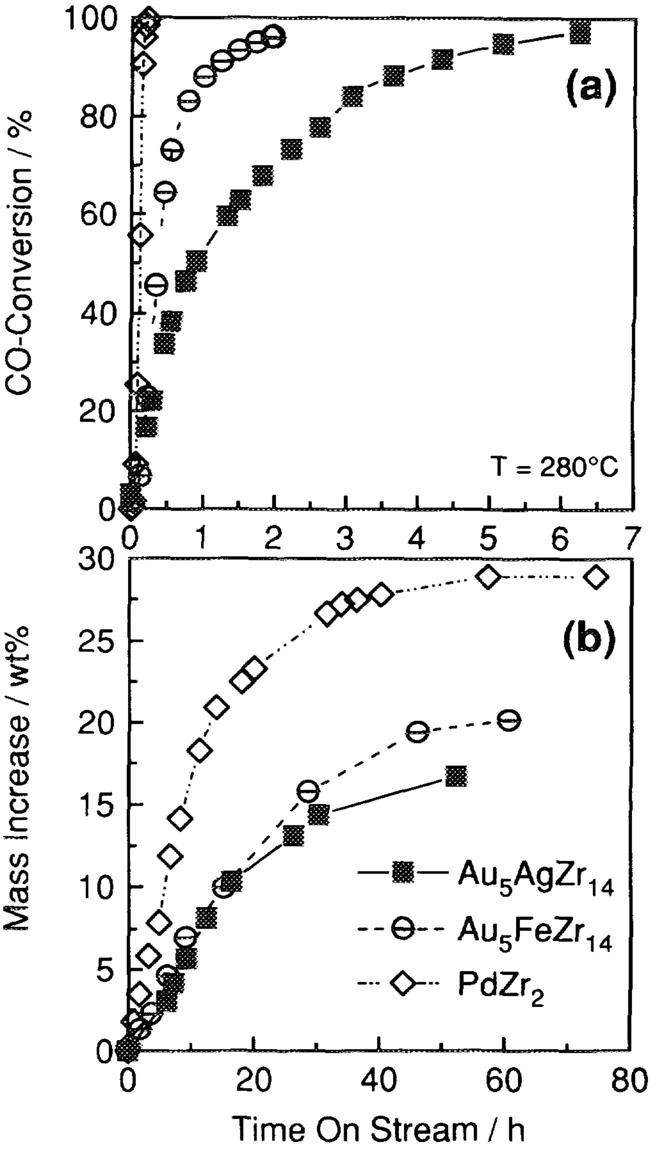

FIG. 3. *In situ* activation of amorphous Au$_5$AgZr$_{14}$ and Au$_5$FeZr$_{14}$ alloys under CO oxidation conditions at 280°C. For comparison corresponding curves for amorphous PdZr$_2$ (16) are also plotted. (a) Development of CO oxidation activity with time on stream; (b) mass increase of metal alloys due to oxidation.

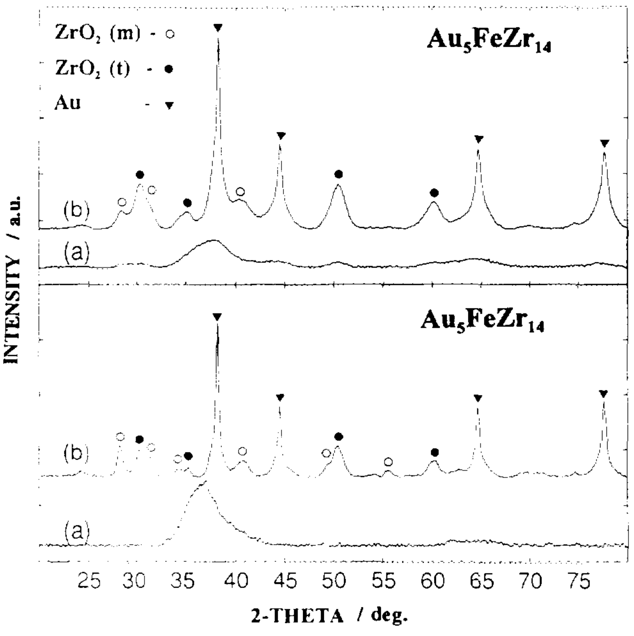

FIG. 4. Powder X-ray diffraction patterns (Cu$K\alpha$) of Au$_5$AgZr$_{14}$ and Au$_5$FeZr$_{14}$ samples before (a) and after activation (oxidation) under CO oxidation conditions (b).

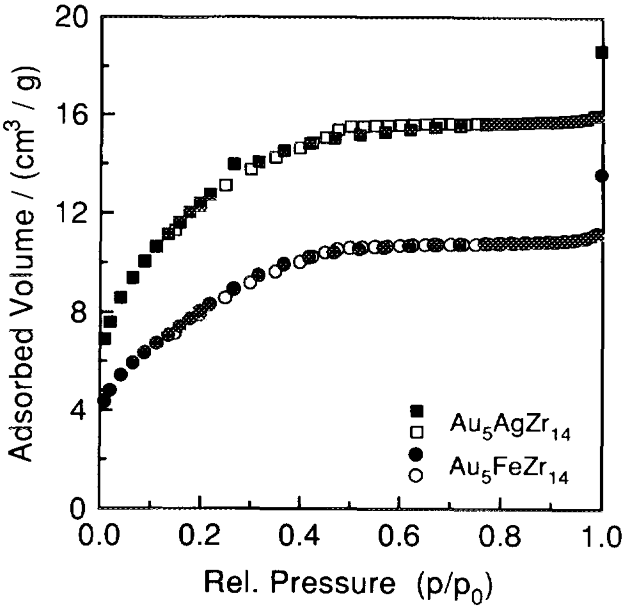

FIG. 5. Nitrogen adsorption (filled symbols) and desorption isotherms (open symbols) of catalysts derived from Au$_5$AgZr$_{14}$ and Au$_5$FeZr$_{14}$ alloys by *in situ* activation at 280°C. Corresponding surface areas and mean pore diameters are listed in Table 1.

The bulk structural changes of the alloys occurring during *in situ* oxidation resulted in a volume expansion and a concomitant change of the textural properties of the solids (Table 1). Note that the BET surface areas of the samples increased by more than three orders of magnitude from <0.02 to 44.7 m^2/g (Au$_5$AgZr$_{14}$) and 29.6 m^2/g (Au$_5$FeZr$_{14}$). The mean gold crystallite size as determined by XRD line broadening was similar for both catalysts (17 and 18 nm, respectively).

Nitrogen adsorption–desorption measurements shown in Fig. 5 yielded type I isotherms (Langmuir type), according to IUPAC nomenclature (17), with no hysteresis between adsorption and desorption branches. This characteristic feature is indicative for the absence of mesopores, which was further confirmed from *t*-plot constructions using the Harkins–Jura correlation (18). Thus the development of the BET surface area is exclusively due to the formation of micropores.

Figures 6 and 7 depict the morphological changes which occurred during the *in situ* oxidation of the glassy alloys, as seen by scanning electron microscopy. The precursor alloy particles, which were obtained by grinding the thin ribbons fabricated by melt spinning under liquid nitrogen, showed a relatively rough surface structure (top plates). The most significant change occurring upon activation (oxidation) was the segregation and formation of small metal particles on the surface. With the Au$_5$AgZr$_{14}$ precursor these particles tended to coalesce to larger agglomer-

TABLE 1

Morphological Properties of the Catalysts Prepared from Amorphous Gold Alloys

Amorphous precusor	Pretreatment	BET surface area (m^2/g)	Mean pore size (nm)	Mean gold crystallite size[a] (nm)
Au$_5$AgZr$_{14}$	*In situ* oxidation at 280°C	44.7	2.1	17
Au$_5$FeZr$_{14}$	(CO oxidation conditions)	29.6	2.3	18
Au$_5$AgZr$_{14}$	Oxidation in air at 240°C	—	—	11
Au$_5$FeZr$_{14}$	Oxidation in air at 225°C	—	—	10

[a] Determined by X-ray diffraction line broadening from the Au (111), (200), and (220) reflections.

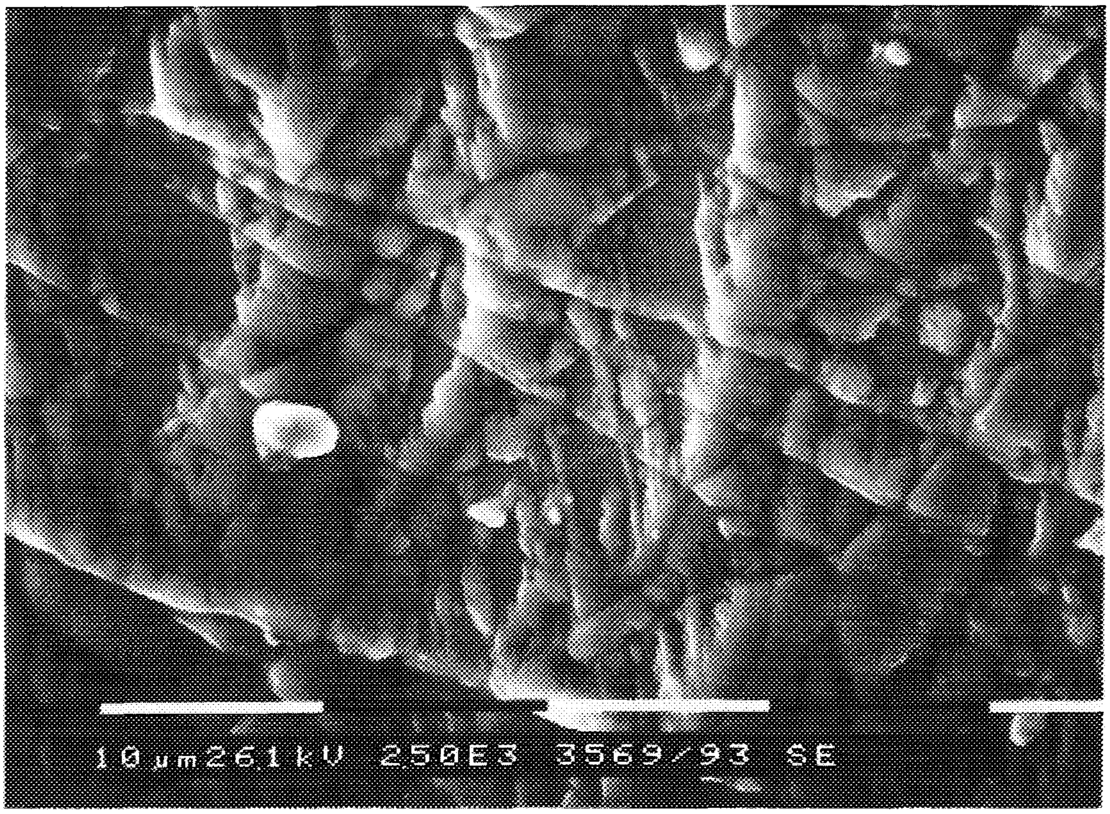
10µm26.1kV 2.50E3 3569/93 SE

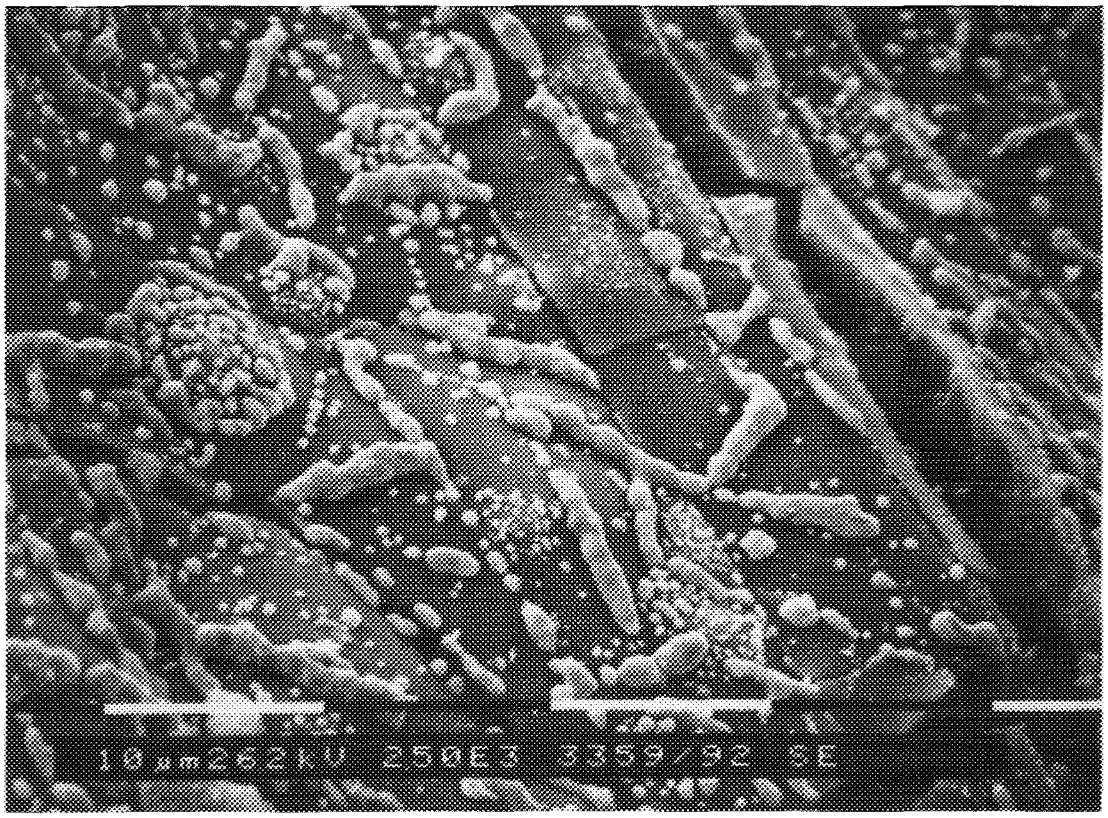
10µm26.2kV 2.50E3 3359/92 SE

ates of various shapes (Fig. 6), whilst with Au_5FeZr_{14} (Fig. 7) this tendency was less pronounced, leading to metal particles of more spherical and regular shape. A comparative energy dispersive X-ray analysis (Fig. 8) of the segregated metal particles and the underlying support material indicated that with the catalyst prepared from Au_5AgZr_{14}, Au and Ag were predominantly contained in the segregated metal particles (compare intensities of Au and Ag peaks in Fig. 8 A and B). A similar comparison made for the catalyst prepared from Au_5FeZr_{14} indicated that the segregated metal particles contained mainly gold and that the iron constituent was accumulated in the underlying matrix. Unfortunately, the limited spacial resolution of EDX did not allow an unambiguous identification of the components contained in the segregated metal particles. However, the EDX results reflect the behaviour which would be expected based on the phase diagrams of Au–Ag (19) and Au–Fe alloys (20), which indicate that the formation of Au–Ag particles is likely, whereas the formation of Au–Fe particles is not expected, particularly if the iron constituent is oxidized, as the subsequently discussed XPS investigation revealed.

Further information concerning the chemical and structural properties of the catalysts was gained by X-ray photoelectron spectroscopy. Analysis of the Zr 3*d* spectra of both catalysts indicated that the zirconium was completely oxidized to ZrO_2 after *in situ* oxidation. Figure 9 (left side) depicts the XP Au 4*f* and Fe 2*p* spectra of the catalyst derived from Au_5FeZr_{14} and the Au 4*f* and Ag 3*d* spectra of the catalyst prepared from Au_5AgZr_{14} (right side). Deconvolution of the Au 4*f* spectra of both catalysts indicated that the spectra were the result of a superposition of two different Au 4*f* spectra, one located at the expected position (Au $4f_{7/2}$ at 84.0 eV and Au $4f_{5/2}$ at 87.6, (21)) and the other one shifted by 1.2 eV to higher binding energies due to charging. The problem of inhomogeneous electrostatic charging and its effect on XPS measurements has been discussed by Muhler *et al.* (22). Based on the structural characteristics of the alloy-derived gold catalysts and the observed shifts in the Au 4*f* spectra, we can distinguish between two types of gold-containing particles: particles which are located in a conductive matrix, and particles which are embedded in an insulating matrix (ZrO_2 matrix). The latter particles are charged and give rise to the Au 4*f* spectra shifted to higher binding energy.

In agreement with scanning electron microscopy (Figs. 6 and 7), the Au 4*f* spectra shown in Fig. 9 indicate that isolated gold particles (in ZrO_2 matrix) are prevalent on the catalyst derived from Au_5FeZr_{14}, whereas larger conductive agglomerates prevail on the catalyst prepared from Au_5AgZr_{14} as indicated in a deconvolution of the spectra. The Fe 2*p* spectrum of the catalyst derived from Au_5FeZr_{14} shows the same shift to higher binding energy (Fe $2p_{3/2}$, 712.6 eV, literature value 711.3 eV (23) as observed with Au 4*f*, indicating that the iron oxide was present exclusively as isolated domains in the zirconia matrix.

The Ag 3*d* spectrum of the catalyst derived from Au_5AgZr_{14} is also made up of two superimposed spectra, one appearing at the expected position (Ag $3d_{5/2}$, 368.3 eV, Ag $3d_{3/2}$, 374.1 eV (21), the other shifted by ca. 1.2 eV to higher binding energy due to charging. The similarity in the splitting of the Au 4*f* and Ag 3*d* spectra is indicative of the formation of Au–Ag particles on this catalyst and provides further evidence for the Au–Ag particle formation indicated by the energy dispersive X-ray analysis (Fig. 8).

From the above investigations, the following conclusions can be made with regard to the morphological and chemical properties of the catalyst prepared by *in situ* activation (oxidation) of the glassy gold-containing alloys. Both catalysts are microporous and contain a mixture of tetragonal and monoclinic zirconia as major components. The catalyst prepared from Au_5FeZr_{14} is made up of gold particles which are supported on an iron-oxide-containing zirconia matrix. The catalyst derived from Au_5AgZr_{14} contains Au–Ag metal particles which are supported on zirconia.

Catalytic Behaviour in CO Oxidation

Figure 10 shows the behaviour of the catalysts derived from the glassy metal alloys by *in situ* oxidation at 280°C (Fig. 3) for CO oxidation at low temperature and with different reactant mixtures ($CO : O_2$ ratios). Note that both catalysts exhibited steady-state activity only after being on stream for several hours. The unsteady-state initial period shows markedly different characteristics. The reason for this behaviour is not yet understood and merits further attention. A common feature of both catalysts is that CO conversion increases with decreasing reactant ratio $CO : O_2$.

Figure 11 depicts the CO conversions measured over both catalysts for ascending (filled circles) and descending (open circles) temperature sequences. Note the significantly higher CO oxidation activity of the catalyst derived from Au_5FeZr_{14}.

FIG. 6. Scanning electron micrographs showing the morphology of the Au_5AgZr_{14} alloy (precursor) and active $Au/Ag/ZrO_2$ catalyst derived from it. Top: amorphous metal alloy precursor; bottom: active catalyst.

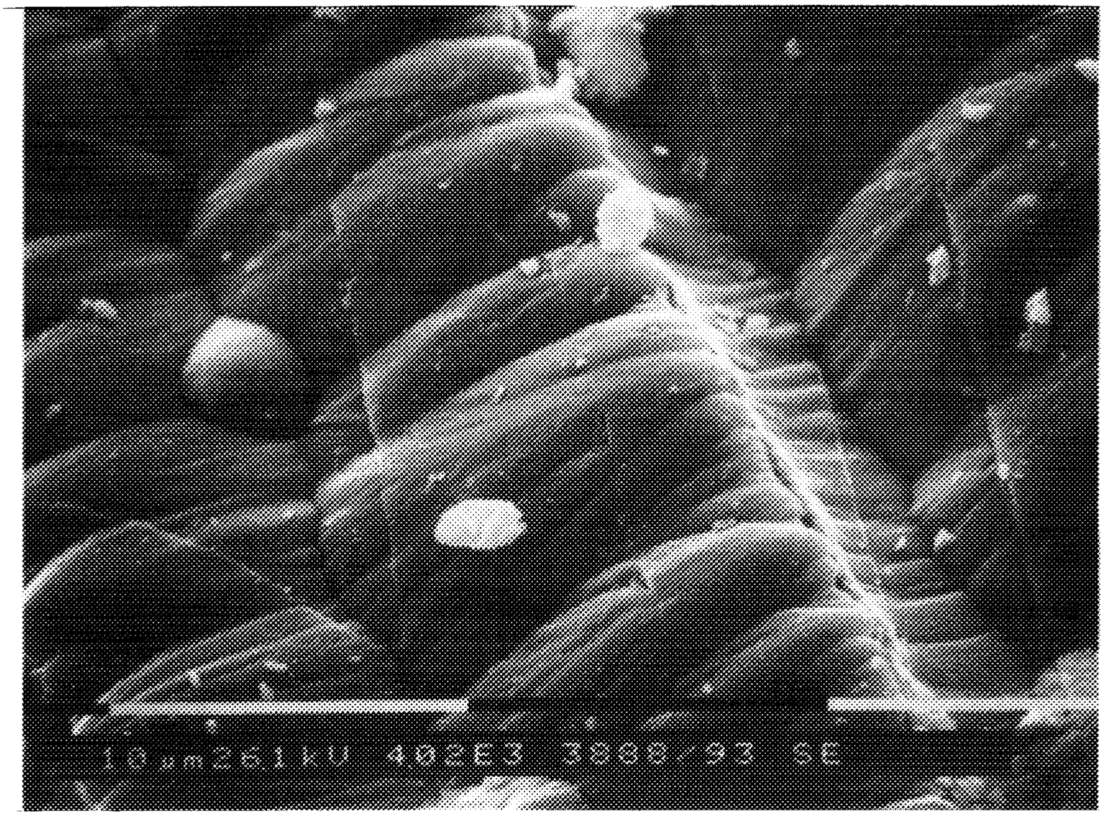
10µm261kV 402E3 3888/93 SE

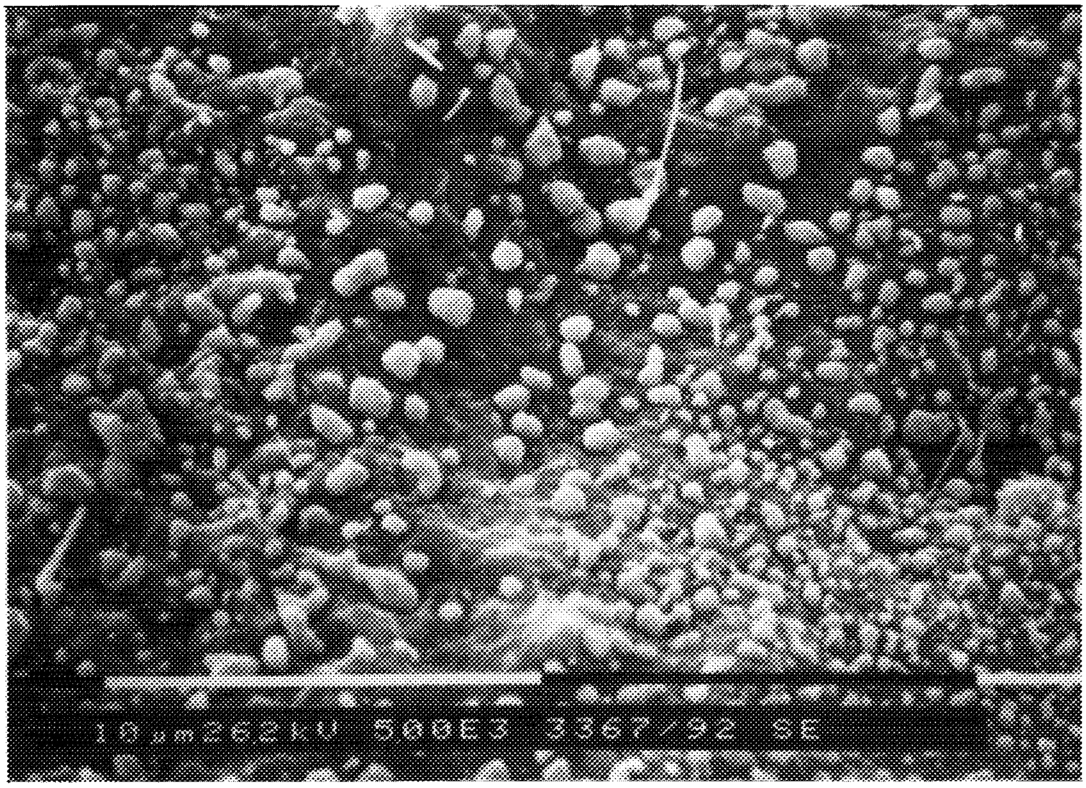
10µm262kV 500E3 3367/92 SE

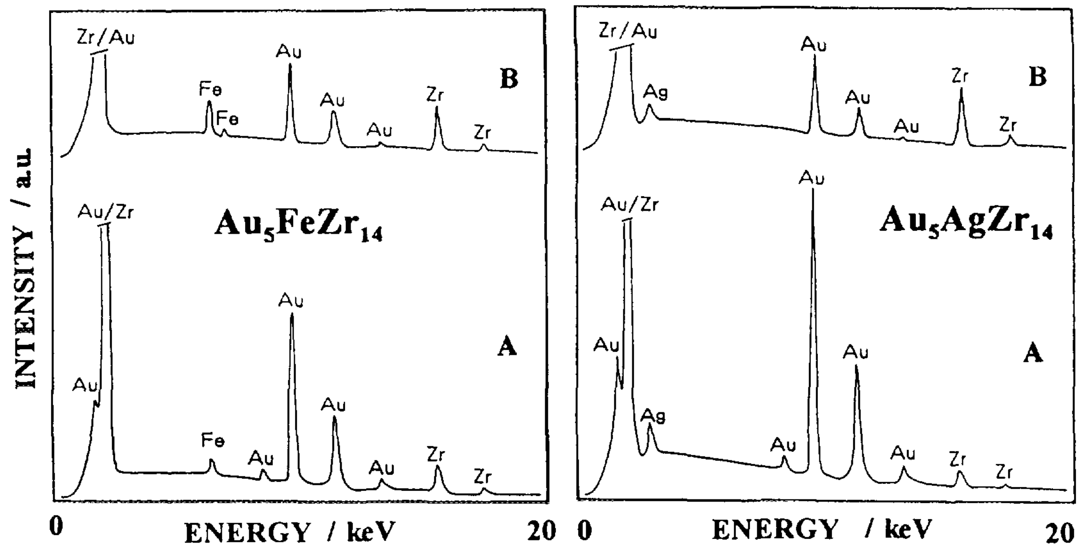

FIG. 8. Energy dispersive X-ray analysis of catalysts prepared from amorphous Au_5AgZr_{14} and Au_5FeZr_{14} shown in scanning electron micrographs presented in Figs. 6 and 7, respectively: (A) analysis of surface metal particles; (B) analysis of support matrix.

The Arrhenius diagrams of CO reaction rates measured for the stable catalysts are plotted in Fig. 12. Note that the rates were measured with ascending (filled symbols) and descending (open symbols) temperature sequences. Both gold-containing catalysts exhibit a significantly higher activity in the low temperature range than a similarly prepared Pd/ZrO_2 catalyst derived from the glassy $PdZr_2$ alloy, as the comparative presentation of the Arrhenius plots reveals. The gold-containing catalysts show markedly different apparent activation energies: gold–zirconia–iron oxide 118 ± 15 kJ/mol; gold–silver–zirconia 84 ± 2 kJ/mol. The activation energy of the catalyst derived from $PdZr_2$ (16) amounted to 86 ± 7 kJ/mol, which is in the middle of the range of activation energies (55–126 kJ/mol) reported for CO oxidation over pure Pd catalysts (24). It should be mentioned at this point that catalysts prepared by *in situ* oxidation under CO oxidation conditions, which were not subjected to reduction under a hydrogen atmosphere before kinetic tests, showed a significantly smaller apparent activation energy (25). This behaviour is attributed to the fact that *in situ* activation results in catalysts which contain PdO, whereas after reduction in a hydrogen atmosphere only metallic Pd is present.

DISCUSSION

When exposed to CO oxidation conditions at 280°C, the amorphous metal alloys exhibit initially only very low activity. This behaviour is attributed to the low surface area of the nonporous glassy metal alloys (<0.03 m^2/g) and to the fact that alloys which contain zirconium as the main component tend to form a passivating zirconia layer on the surface. This phenomenon has been observed with Cu–Zr (26), Fe–Zr (27), Ni–Zr (28), and Pd–Zr (29) alloys. Concentration depth profile measurements indicated that the surface region is enriched with the zirconium component due to zirconium segregation and subsequent reaction with oxygen to zirconia.

The oxidation of the zirconium to ZrO_2 during exposure to the reaction conditions is crucial for the development of the CO oxidation activity. This emerges clearly from the simultaneous monitoring of the weight gain of the alloys due to oxidation and the concomitant development of the activity shown in Fig. 3. The zirconium constituent is oxidized to stoichiometric ZrO_2 as was confirmed by XPS analysis. It is noteworthy to mention at this point that with similarly oxidized Pd–Zr the presence of nonstoichiometric, oxygen-deficient zirconia ZrO_{2-x} has been found by XPS (29).

With both alloys the zirconium component is transformed to a mixture of poorly crystalline tetragonal and monoclinic zirconia (Fig. 4). This indicates that the phase composition is largely kinetically controlled, since the thermodynamically more stable phase is the monoclinic phase under the conditions applied (30).

The oxidation of the zirconium constituent leads to

FIG. 7. Scanning electron micrographs showing the morphology of the Au_5FeZr_{14} alloy (precursor) and active Au/ZrO_2–Fe_2O_3 catalyst derived from it. Top: amorphous metal alloy precursor; bottom: active catalyst.

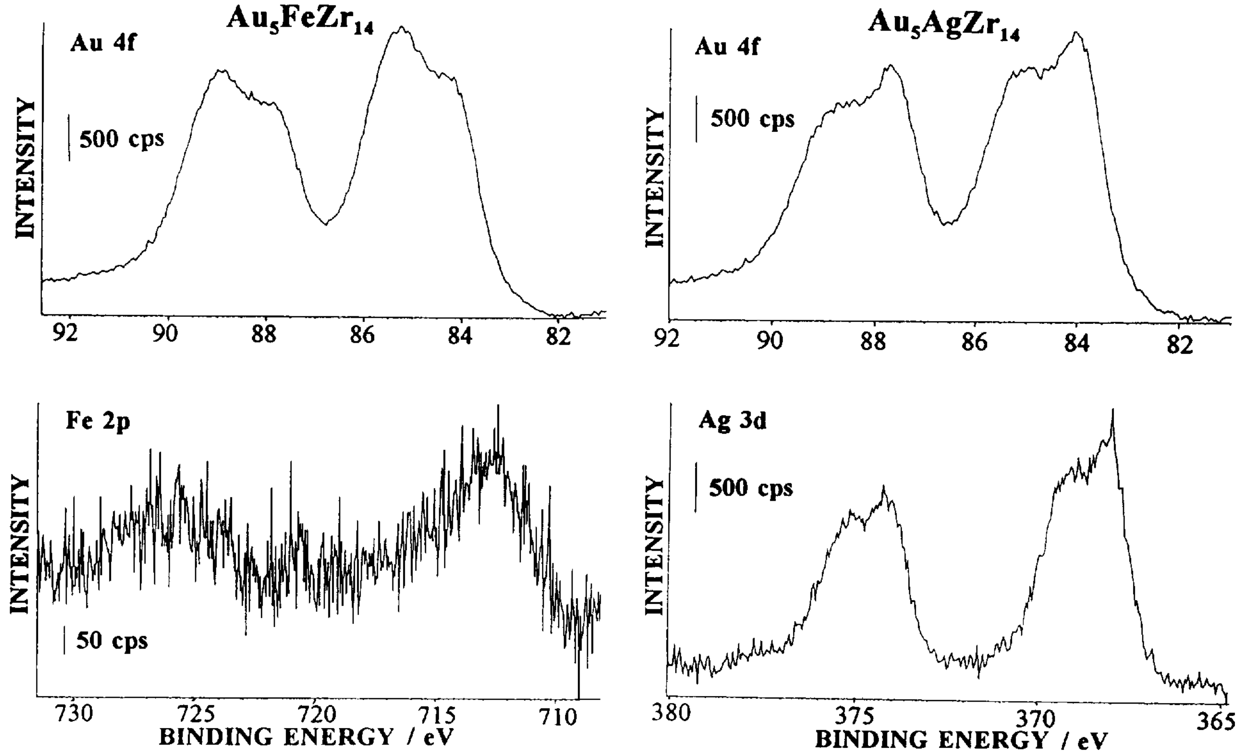

FIG. 9. Au 4*f* and Fe 2*p* XP spectra measured for catalyst derived from Au_5FeZr_{14} (left side) and Au 4*f* and Ag 3*d* XP spectra measured for catalyst prepared from Au_5AgZr_{14} (right side). Zr 3*d* spectra (not shown) were similar for both catalysts indicating complete oxidation of Zr to ZrO_2.

a drastic expansion of the volume of the alloys and to considerable interfacial strain which is responsible for the creation of cracks and the build-up of pores and internal surface area. The increase in the BET surface areas (Table 1) by more than three orders of magnitude is crucial for the development of the activity. Another important factor for the activation is the enrichment of the Group IB metals (gold and silver) on the surface, which requires the segregation of these constituents from the bulk of the solid material onto the surface. At 280°C (temperature of activation) the formation of intermetallic compounds between IB metals (gold and silver) and zirconium (31) seems kinetically rather unlikely; nucleation and growth of IB metal crystallites is supposed to dominate, thus leading to a metastable equilibrium between the crystalline IB metals and the nonoxidized metallic zirconium. The low temperature and low diffusion rate of Zr (32), compared to that of Au and Ag, exclude the formation of IB metal–zirconium equilibrium phases.

Figure 13 summarizes schematically the main differences in the structural features of the catalysts derived from the amorphous Au_5AgZr_{14} and Au_5FeZr_{14} alloys. Although several features of the genesis of the catalysts are common for both alloys, there are distinct differences in the structural properties caused by the nature of the third components (silver and iron, respectively) in these alloys. The iron constituent in Au_5FeZr_{14} is oxidized to iron oxide (probably Fe_2O_3) which seems to be stable under CO oxidation conditions, whereas silver in the Au_5AgZr_{14} precursor forms a solid solution with gold (19) as suggested by the EDX and XPS investigations. The small gold–silver particles tend to coalesce to larger agglomerates (Fig. 6), whereas the gold particles on the catalyst derived from Au_5FeZr_{14} remain significantly better dispersed (Fig. 7). Although Au and Fe are also known to be able to form a solid solution (20), this is impossible under the present conditions due to the rapid oxidation of Fe under the activation conditions applied.

The catalysts prepared from both alloys show high activity for CO oxidation at low temperature and are stable during experiments after about 40 h on stream (Fig. 10). Similar long-term stability has not been observed with gold-zirconia catalysts prepared by coprecipitation (10). With both alloy-derived catalysts the steady-state conversion is higher with reactant mixtures corresponding to a $CO : O_2$ ratio of 1 : 2, indicating that excess oxygen is beneficial.

The gold–silver–zirconia and gold–zirconia–iron oxide catalysts exhibit considerably higher activity at low temperature than a similarly prepared Pd/ZrO_2 catalyst, as emerges from the comparative presentation of the Arrhenius plots in Fig. 12. The catalysts derived from Au_5FeZr_{14}

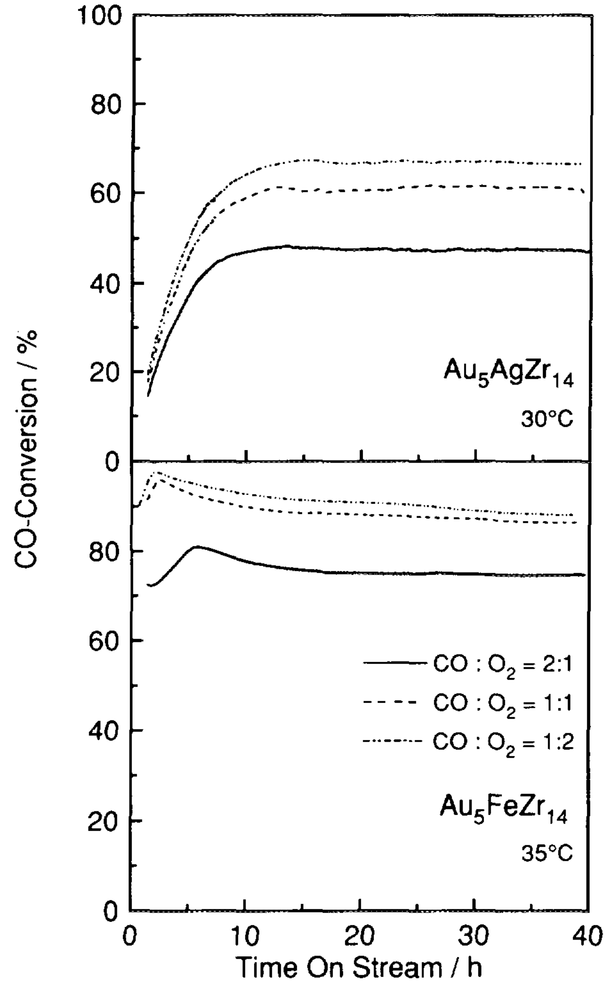

FIG. 10. Behaviour of catalysts derived from glassy Au_5AgZr_{14} and Au_5FeZr_{14} alloys by *in situ* activation at 280°C (Fig. 3). CO conversion is plotted versus time on stream for reaction at low temperature (30 and 35°C, respectively) and with different stoichiometry of reactant mixture. Different stoichiometries were achieved by varying the oxygen partial pressure, whereas the CO partial pressure was kept constant at 0.17 kPa. Other conditions are specified under Experimental.

is significantly more active than that prepared from Au_5AgZr_{14}. The reaction rates referring to the gold metal content hint towards gold being more active in the gold–zirconia–iron oxide than in the gold–silver–zirconia. Silver seems to have no promoting effect for CO oxidation in gold–zirconia catalysts. However, further investigations are necessary before a conclusive answer can be given about the effect of silver on the CO oxidation activity of gold.

The activation energies (gold–zirconia–iron oxide, 118 kJ/mol; gold–silver–zirconia, 84 kJ/mol) calculated from the Arrhenius plots indicate that intraparticle diffusion limitation of the measured reaction rates is unlikely. The activation energies of our zirconia-based gold catalysts are considerably higher than those reported by Lin *et al.* (9) for Au/TiO_2 (0–13 kJ/mol, depending on pretreatment) and Au/SiO_2 (15 kJ/mol) prepared by an incipient wetness method (9) and also higher than those found for Au/TiO_2 (35 kJ/mol), $Au/\alpha\text{-}Fe_2O_3$ (35 kJ/mol), and Au/Co_3O_4 (16 kJ/mol) by Haruta and co-workers (8). This indicates that the nature of the active sites may be different on the catalysts prepared from the glassy metal alloys.

Unfortunately, no conclusive comparison of the activities of our gold–zirconia catalysts with other gold-based catalysts reported in the literature (8, 9) can be made, due to the very different reaction conditions and catalyst pretreatments which were used in the kinetic tests. Lin *et al.* (9) used about 30 times higher reactant concentrations and a much lower space velocity than we used in the present work. Haruta *et al.* (8) used an extremely large excess of oxygen. Only a direct comparison of the activities of all these catalysts measured under the same reaction conditions would allow us to rank the different gold catalysts according to their activity. However, a direct comparison of the activities of the catalysts prepared in this work and Au/ZrO_2 investigated in our previous work (10) is possible, since similar reaction conditions were applied. Comparing the reaction rates [μmol CO/g_{Au} s)] for these catalysts at 0°C we find 0.75 for Au/ZrO_2 (10), 0.59 for the catalyst prepared from Au_5FeZr_{14}, and 0.13 for the catalysts prepared from Au_5AgZr_{14}. The comparison reveals that the gold metal atoms in the highly loaded gold catalyst prepared from Au_5FeZr_{14} (35.4 wt.%) are almost as efficiently used as those in the conventionally prepared Au/ZrO_2 catalyst (10) which contained 15.1 wt% Au. A decisive advantage of the alloy-derived gold catalysts compared with the coprecipitated Au/ZrO_2 catalyst is that no catalyst deactivation was observed. Whether this resistance to deactivation is also observed with catalysts derived from similar alloys with lower gold content remains to be proven.

Finally it should be mentioned that the conditions used for the activation (oxidation) of the amorphous metal alloys have not as yet been optimized and consequently further improvement of the activity of as-prepared catalysts seems possible. How critical the pretreatment conditions can be for the final performance of gold-based catalysts has been demonstrated recently (9, 33). Possible further improvement of the alloy-derived gold catalysts is indicated by thermogravimetric activation (oxidation) studies carried out at lower temperature and in air. These procedures lead to mean gold crystallite sizes which were remarkably smaller (~10 nm compared to 18 nm with *in situ* oxidation, Table 1).

CONCLUSIONS

Gold–metal oxide catalysts, highly active for the low-temperature oxidation of carbon monoxide, can be pre-

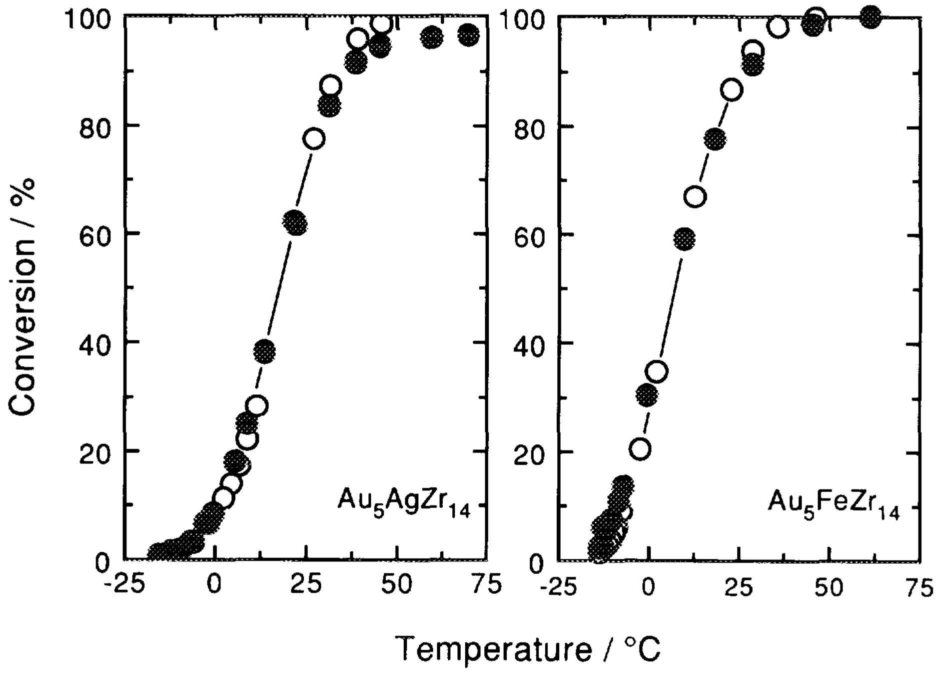

FIG. 11. Temperature dependence of CO oxidation over catalysts derived from Au_5AgZr_{14} and Au_5FeZr_{14} alloys measured in series of measurements with ascending (filled circles) and descending (open circles) temperature. Each data point represents CO conversion after steady state was achieved.

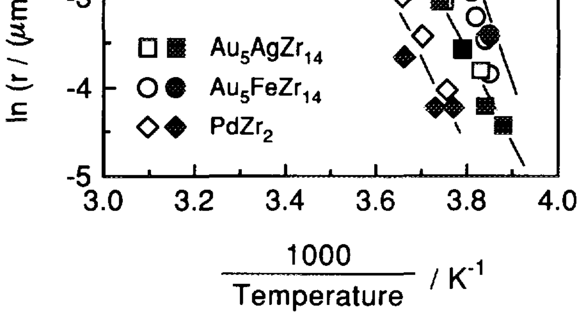

FIG. 12. Arrhenius diagrams of CO reaction rates measured for catalysts derived from Au_5AgZr_{14} and Au_5FeZr_{14} alloys by *in situ* activation (oxidation) at 280°C. Filled symbols represent data measured with ascending temperature sequence and open symbols data measured with descending temperature, respectively. The Arrhenius line measured for a similarly activated amorphous $PdZr_2$ alloy is plotted for comparison.

pared by *in situ* oxidation of glassy metal alloys of the compositions Au_5FeZr_{14} and Au_5AgZr_{14} at 280°C, a temperature greatly below the crystallization temperatures of the alloys (>500°C). Upon exposure of the alloys to CO oxidation conditions at 280°C, the initially low activity of the materials increases drastically. The increase in the activity is accompanied by drastic structural and chemical changes of the alloys. The zirconium constituent is oxidized to ZrO_2 and the gold segregates onto the surface

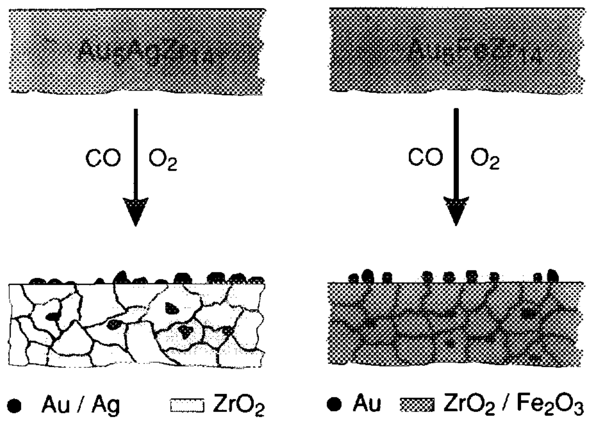

FIG. 13. Schematic representation of structural characteristics of catalysts derived by *in situ* activation (oxidation) of glassy Au_5AgZr_{14} and Au_5FeZr_{14} alloys.

forming crystallites of 17–18 nm mean size. Iron in the catalysts derived from Au_5FeZr_{14} is present as iron oxide which is distributed in the zirconia matrix. Silver contained in the catalyst prepared from Au_5AgZr_{14} forms a solid solution with gold resulting in gold–silver particles on the catalyst surface. The final microporous gold–zirconia–iron oxide and gold–silver–zirconia catalysts are highly active at ambient temperature and exhibit stable activity, as proven by tests over 40 h.

ACKNOWLEDGMENT

Thanks are due to Alusuisse-Lonza AG, Switzerland for supporting this work.

REFERENCES

1. Schwank, J., *Gold Bull.* **16,** 103 (1983).
2. Bone, W. A., and Andrew, G. W., *Proc. R. Soc. (London) A* **109,** 459 (1925).
3. Daglish, A. G., and Eley, D. D., *Proceedings, 2nd International Congress on Catalysis*, Vol. 2, p. 1615 1961.
4. Cha, D. Y., and Parravano, G., *J. Catal.* **18,** 200 (1970).
5. Galvagno, S., and Parravano, G., *Ber. Bunsenges. Phys. Chem.* **83,** 894 (1979).
6. Cant, N. W., and Fredrickson, P. W., *J. Catal.* **37,** 531 (1975).
7. Haruta, M., Yamada, N., Kobayashi, T., and Iijima S., *J. Catal.* **115,** 301 (1989).
8. Haruta, M., Tsubota, S., Kobayashi, T., Kageyama, H., Genet, M. J., and Delmon, B., *J. Catal.* **144,** 175 (1993).
9. Lin, S. D., Bollinger, M., and Vannice, M. A., *Catal. Lett.* **17,** 245 (1993).
10. Knell, A., Barnickel, P., Baiker, A., and Wokaun, A., *J. Catal.* **137,** 306 (1992).
11. Gardner, S. D., Hoflund, G. B., Upchurch, B. T., Schryer, D. R., and Kielin, E. J., *Langmuir* **7,** 2135 (1991).
12. Kobayashi, T., Haruta, M., Sano, H., and Nakane, M., *Sensors and Actuators* **13,** 339 (1988).
13. JCPDS Mineral Powder Diffraction Data Files, Park Lane, Pennsylvania.
14. Guilliatt, I. F., and Brett, N. H., *J. Brit. Ceram. Soc.* **6,** 56 (1969).
15. Baiker, A., *in* "Topics in Applied Physics," (H. Beck and H. J. Güntherodt, Eds.), Vol. 72, p. 121, Springer-Verlag, Berlin, 1994.
16. Baiker, A., Maciejewski, M., and Tagliaferri, S., *Ber. Bunsenges. Phys. Chem.* **97,** 286 (1993).
17. Sing, K. S. W., Everett, D. H., Haul, R. A. W., Moscou, L., Pierotti, R. A., Rouquerol, J., and Siemieniewska, T., *Pure Appl. Chem.* **57,** 603 (1985).
18. Harkins, W. D., and Jura, G. J., *J. Chem. Phys.* **11,** 431 (1943).
19. Cooke, C. J., and Hume-Rothery, W., *Acta Metall.* **9,** 982 (1961).
20. Okamoto, H., Massalski, T. B., Swartzendruber, L. J., and Beck, P. A., *Bull. Alloy Phase Diagrams* **5,** 258 (1984).
21. Briggs, D. and Shea, M. P., "Practical Surface Analysis," Wiley Chichester, NY, 1988.
22. Muhler, M., Paál, Z., and Schlögl, R., *Appl. Surf. Sci.* **47,** 281 (1991).
23. McIntyre, N. S., and Zetaruk, D. G., *Anal. Chem.* **49,** 1521 (1977).
24. Yu Yao, Y. F., *J. Catal.* **28,** 1 (1979).
25. Baiker, A., Gasser, D., Lenzner, J., Reller, A., and Schlögl, R., *J. Catal.* **126,** 555 (1990).
26. Baiker, A., Baris, H., Erbudak, M., and Vanini, F., *in* "Proceedings 9th International Congress on Catalysis, (M. J. Phillips and M. Ternan, Eds.), p. 1928. Chem. Inst. Can., Ottawa, 1988.
27. Baiker, A., Schlögl, R., Armbruster, E., and Güntherodt, H-J., *J. Catal.* **107,** 221 (1987).
28. Walz, B., Oelhafen, P., Güntherodt, H-J., and Baiker, A., *Appl. Surf. Sci.* **37,** 337 (1989).
29. Schlögl, R., Loose, G., Wesemann, M., and Baiker, A., *J. Catal.* **137,** 139 (1992).
30. Subbaro, E. C., *in* "Advances in Ceramics" (A. H. Heuer and L. W. Hobbs, Eds.), Vol. 3, p. 1. Am. Ceram. Soc., Columbus, Ohio, 1981.
31. Stolz, E., and Schubert, K., *Z. Metallkd.* **53,** 433 (1962).
32. Cahn, R. W., *in* "Physical Metallurgy" 3rd ed. (R. W. Cahn and P. Haasen, Eds.), p. 1779. Elsevier, Amsterdam, 1983.
33. Tanielyan, S. K., and Augustine, R. L., *Appl. Catal. A: General* **85,** 73 (1992).